JACS
JOURNAL OF THE AMERICAN CHEMICAL SOCIETY

Subscriber access provided by American Chemical Society

View the Full Text HTML

ACS Publications
High quality. High impact.

Journal of the American Chemical Society is published by the American Chemical Society. 1155 Sixteenth Street N.W., Washington, DC 20036

J|A|C|S
ARTICLES
Published on Web 03/10/2006

Nature of the Bottom t_{2g}-Block Bands of Layered Perovskites. Implications for the Transport Properties of Phases Where These Bands Are Partially Filled

Gerard Tobias† and Enric Canadell*

Contribution from the Institut de Ciència de Materials de Barcelona (CSIC), Campus de la UAB, 08193 Bellaterra, Spain

Received October 25, 2005; E-mail: canadell@icmab.es.

Abstract: The electronic structure of a series of double layer ($Sr_3V_2O_7$, $KLaNb_2O_7$, $Li_2SrNb_2O_7$, $RbLaNb_2O_7$, $Rb_2LaNb_2O_7$) as well as triple layer ($Ca_4Ti_3O_{10}$, $K_2La_2Ti_3O_{10}$, $Sr_4V_3O_{9.7}$, $CsCa_2Nb_3O_{10}$) Dion−Jacobson and Ruddlesden−Popper phases and quadruple layer $A_nB_nO_{3n+2}$ phases ($Sr_2Nb_2O_7$ as well as the low-temperature and room-temperature structures of $Sr_2Ta_2O_7$) has been studied by means of a first-principles density functional theory approach. The results are rationalized on the basis of a simple tight-binding scheme, which provides a simple yet precise scheme allowing the correlation of the crystal structure details and the nature of the bottom t_{2g}-block band levels. Both the quantitative and the qualitative approaches are used to analyze the nature of the carriers in intercalated samples of the d^0 semiconducting phases as well as those of the metallic d^x ($0 < x \leq 1$) systems. The Ruddlesden−Popper and Dion−Jacobson materials with partially filled t_{2g}-block bands must be genuine two-dimensional metals except when the M−O_{ap} distances of the outer layer octahedra are similar and the band filling is not low. The conducting electrons in these phases are almost equally distributed among the different layers. It is shown that the $A_nB_nO_{3n+2}$ phases with partially filled bands are potentially interesting materials because they are structurally two-dimensional materials exhibiting one-dimensional band structure features. Finally, the possible application of the simple scheme to related materials such as layered perovskite oxynitrides and the effect of disorder are briefly discussed.

Introduction

Chemical intercalation in low-dimensional materials has long been a convenient approach to modify their transport properties. Essentially, intercalation offers the possibility of controlling (at least partially) the filling of the bands that dominate the transport and other collective properties of the material. Thus, from this viewpoint, it can be a powerful tool in inducing property changes while keeping the essential structural details of the solid or in testing theories of physical phenomena in these materials. There is a vast literature on the subject, and many interesting materials (graphite, transition metal oxides, and chalcogenides, etc.) have been carefully studied along this line.[1] The now celebrated discovery of high-T_c superconductivity[2] launched an enormous interest in the chemistry and physics of doped layered materials, and as a result new solids of this type exhibiting remarkable transport properties have been prepared. Special mention among those that have recently been the object of much interest and debate is given to the intercalated zirconium and hafnium nitride halides[3] and the Na_xCoO_2 phases.[4]

The observation of superconductivity in Li_xNbO_2[5a] and Sr_2RuO_4[5b] soon made clear that non-copper superconducting layered oxides could be prepared, and layered perovskites became the focus of a large effort. The Ruddlesden−Popper[6] (R−P) and Dion−Jacobson phases[7] (D−J) are two of the better studied families of these materials. These phases, with general formulas $A_2'[A_{n-1}B_nO_{3n+1}]$ and $A'[A_{n-1}B_nO_{3n+1}]$, where n indicates the thickness of the octahedral slabs (i.e., the number of octahedral layers in a slab), can be formally obtained from the ideal cubic perovskite structure ABO_3 when a cut along the ⟨100⟩ direction is performed (the Aurivillius family of phases can also be formally generated in that way).[8] When the cut is carried out along the ⟨110⟩ direction, a different family with

† Present address: Inorganic Chemistry Laboratory, University of Oxford, South Parks Road, Oxford OX1 3QR, United Kingdom.

(1) (a) Dresselhaus, M. S.; Dresselhaus, G. *Adv. Phys.* **1981**, *30*, 139−326. (b) Rouxel, J. *Ber. Bunsen-Ges. Phys. Chem.* **1989**, *93*, 1219−1224. (c) Jacobson, A. J. In *Solid State Chemistry: Compounds*; Cheetham, A. K., Day, P., Eds.; Oxford University Press: Oxford, 1992; pp 182−233. (d) Whittingham, M. S. *Prog. Solid State Chem.* **1978**, *12*, 41−99. (e) O'Hare, D. In *Inorganic Materials*; Bruce, D. W., O'Hare, D., Eds.; John Wiley: Chichester, 1992; pp 165−235.
(2) Bednorz, J. G.; Müller, A. Z. *Phys. B* **1986**, *64*, 189−193.
(3) (a) Yamanaka, S.; Hohetama, K.; Kawaji, H. *Nature* **1998**, *392*, 580−582. (b) Fuertes, A.; Vlassov, M.; Beltrán-Porter, D.; Alemany, P.; Canadell, E.; Casañ-Pastor, N.; Palacín, M. R. *Chem. Mater.* **1999**, *11*, 203−206. (c) Fogg, A. M.; Green, V. M.; O'Hare, D. *Chem. Mater.* **1999**, *11*, 216−217.
(4) (a) Tanaka, K.; Sakurai, H.; Takayama-Muromachi, E.; Izumi, F.; Dilanian, R. A.; Sasaki, T. *Nature* **2003**, *422*, 53−55. (b) Tanaka, K.; Sakurai, H.; Takayama-Muromachi, E.; Izumi, F.; Dilanian, R. A.; Sasaki, T. *Adv. Mater.* **2004**, *16*, 1901−1905.
(5) (a) Gesselbracht, M. J.; Richardson, T. J.; Stacy, A. M. *Nature* **1990**, *345*, 324−326. (b) Maeno, Y.; Hashimoto, H.; Yoshida, K.; Nishizaki, S.; Fujita, T.; Bednorz, J. G.; Lichtenberg, F. *Nature* **1994**, *372*, 532−534.
(6) Ruddlesden, S. N.; Popper, P. *Acta Crystallogr.* **1958**, *11*, 54−55.
(7) (a) Dion, M.; Ganne, M.; Tournoux, M. *Mater. Res. Bull.* **1981**, *16*, 1429−1435. (b) Jacobson, A. J.; Johnson, J. W.; Lewandowski, J. T. *Inorg. Chem.* **1985**, *24*, 3727−3729.
(8) Levin, I.; Bendersky, L. A. *Acta Crystallogr.* **1999**, *B55*, 853−866.

10.1021/ja0572755 CCC: $33.50 **© 2006 American Chemical Society**

formula $A_nB_nO_{3n+2}$ results.[8] Because the R−P, D−J, and Aurivillius phases all possess the $A_{n-1}B_nO_{3n+1}$ common block, there is a rich set of topochemical processes, which allows interconversions among these structures.[9] Many of these phases are band gap semiconductors, but when their lower t_{2g}-block bands are partially filled because of the intercalation (i.e., the formal configuration of the transition metal atoms is between d^0 and d^1), the possibility of metallic behavior (and superconductivity) occurs. This area has always been quite active, but the reports of superconductivity in the Li-intercalated triple layer phase $Li_xKCa_2Nb_3O_{10}$[10] triggered the attention of many groups toward these layered perovskites. More intriguingly, the double layer Li-intercalated phase $Li_xKLaNb_2O_7$ was found to be metallic but did not exhibit superconductivity down to 0.5 K.[10a] Subsequent work showed that other triple layer perovskites exhibit superconductivity upon chemical or electrochemical Li intercalation.[11] In contrast, superconductivity has not been reported to date in the lithium-intercalated double or quadruple layer systems. This points out the possible control of superconductivity by the layer thickness.

Layered materials of these types with d^x ($0 < x \leq 1$) transition metals can also be directly prepared by solid-state synthesis, with no need of further intercalation, and different approaches have been used toward this end. Single layer $Sr_2NbO_{4-x}N_x$ ($x \approx 0.72$),[12] double layer $Rb_2LaNb_2O_7$,[13] quadruple layer $RbCa_2Na_{1-x}Sr_xNb_4O_{13}$,[14] or the $Sr_{n+1}V_nO_{3n+1}$ ($n = 1, 2, 3, \infty$) family of phases[15] are just some representative examples. However, partial filling of the lower t_{2g}-block bands is not a warranty of metallic behavior. For instance, $Sr_2NbO_{4-x}N_x$ ($x \approx 0.72$)[12] or $Na_{2-x+y}Ca_{x/2}La_2Ti_3O_{10}$ ($x = 1.22$, $y = 0.32$),[16] two phases for which different strategies have been followed to fill the lower part of the t_{2g}-block bands, or the n-doped $HLaNb_2O_7$[17] all exhibit activated conductivity. Interestingly, the $Sr_{n+1}V_nO_{3n+1}$ phases with $n \geq 2$ are metallic, whereas that with $n = 1$ exhibits activated conductivity,[15] something that has not yet been adequately understood.[18] Clearly, several competing electronic effects must occur in layered perovskites with d^x ($0 < x \leq 1$) transition metals.

From just the few examples noted above, it becomes clear that an important step in this field would be the knowledge of the nature of the bottom t_{2g}-block bands of these materials as a function of the type of perovskite phase, transition metal nature and/or configuration, type of cation A, different local octahedral distortions, band filling, etc. Surprisingly, few theoretical works along this line have been reported. We note some extended Hückel works concerning the nature of the FS of Aurivillius-type perovskites as a function of the electron filling[19] and the electronic structure of double layer vanadium and niobium perovskites.[20] Worth mentioning among the first-principles studies is a report concerning $RbLaNb_2O_7$[21] (but using an idealized structure), some brief notes on Sr_2VO_4,[22] as well as two works concerning one of the $A_nB_nO_{3n+2}$ phases.[23] However, the nature of the t_{2g}-block bands was not discussed in the first-principles works, neither was the possible role of cations considered in the extended Hückel ones. Here, we would like to report a detailed study of the nature of the bottom t_{2g}-block bands of layered perovskites with d^x ($0 \leq x \leq 1$) transition metals based on accurate first-principles calculations. We will consider different phases of the R−P, D−J, and $A_nB_nO_{3n+2}$ families chosen so as to provide a picture as broad as possible of the problem at hand. Nevertheless, such a study can only be of real value if it leads to a simple yet trustable model, which can provide explanations and suggest new materials. Our goal is to provide both such a simple conceptual scheme and accurate calculations to explore the correlation between the nature of the low-lying t_{2g}-block bands and structural and electronic variations that can be found in layered perovskites.

Computational Details

The first-principles calculations were carried out using a numerical atomic orbitals density functional theory (DFT) approach,[24] which has been recently developed and designed for efficient calculations in large systems and implemented in the SIESTA code.[25−27] The use of atomic orbitals instead of plane waves greatly facilitates a chemical analysis of the results. We have used the generalized gradient approximation to DFT and, in particular, the functional of Perdew, Burke, and Ernzerhof.[28] Only the valence electrons are considered in the calculation, with the core being replaced by norm-conserving scalar relativistic pseudopotentials[29] factorized in the Kleinman−Bylander form.[30] Nonlinear partial core corrections to describe the exchange and correlations

(9) Schaak, R. E.; Mallouk, T. E. *Chem. Mater*. **2002**, *14*, 1455−1471.
(10) (a) Takano, Y.; Takayanagi, S.; Ogawa, S.; Yamadaya, T.; Môri, N. *Solid State Commun.* **1997**, *103*, 215−217. (b) Takano, Y.; Taketomi, H.; Tsurumi, H.; Yamadaya, T.; Môri, N. *Physica B* **1997**, *237*−*238*, 68−70. (c) Fukuoka, H.; Isasi, T.; Yamanaka, S. *Chem. Lett*. **1997**, 703−704.
(11) (a) Takano, Y.; Kimishima, Y.; Yamadaya, T.; Ogawa, S.; Môri, N. *Rev. High Pressure Sci. Technol*. **1998**, *7*, 589−591. (b) Nagai, I.; Abe, Y.; Kato, M.; Koike, Y.; Kakihana, M. *Physica C* **2001**, *357*−*360*, 393−396. (c) Nagai, I.; Abe, Y.; Kato, M.; Koike, Y.; Kakihana, M. *Solid State Ionics* **2002**, *151*, 265−268. (d) Kato, M.; Inoue, A.; Nagai, I.; Kakihana, M.; Sleight, A. W.; Koike, Y. *Physica C* **2003**, *388*−*389*, 445−446.
(12) (a) Tobias, G.; Oró-Solé, J.; Beltrán-Porter, D.; Fuertes, A. *Inorg. Chem.* **2001**, *40*, 6867−6869. (b) Tobias, G.; Beltrán-Porter, D.; Lebedev, O. I.; Van Tendeloo, G.; Rodríguez-Carvajal, J.; Fuertes, A. *Inorg. Chem.* **2004**, *43*, 8010−8017.
(13) Armstrong, A. R.; Anderson, P. A. *Inorg. Chem*. **1994**, *33*, 4366−4369.
(14) Sugimoto, W.; Ohkawa, H.; Naito, M.; Sugahara, Y.; Kuroda, K. *J. Solid State Chem*. **1999**, *148*, 508−512.
(15) Nozaki, A.; Yoshikawa, H.; Wada, T.; Yamauchi, H.; Tanaka, S. *Phys. Rev. B* **1991**, *43*, 181−185.
(16) Lalena, J. N.; Cushing, B. L.; Falster, A. U.; Simmons, W. B.; Seip, C. T.; Carpenter, E. E.; O'Connor, C. J.; Wiley, J. B. *Inorg. Chem*. **1998**, *37*, 4484−4485.
(17) (a) Gómez-Romero, P.; Palacín, M. R.; Casañ, N.; Fuertes, A. *Solid State Ionics* **1993**, *63*−*65*, 424−428. (b) Palacín, M. R.; Lira, M.; García, J. L.; Caldés, M. T.; Casañ-Pastor, N.; Fuertes, A.; Gómez-Romero, P. *Mater. Res. Bull*. **1996**, *31*, 217−225.
(18) For a detailed discussion of the metallic versus insulating states in perovskites such as $SrVO_3$, $YTiO_3$, and $LaTiO_3$, see: (a) Pavarini, E.; Biermann, S.; Poteryaev, A.; Lichtenstein, A. I.; Georges, A.; Andersen, O. K. *Phys. Rev. Lett.* **2004**, *92*, 176403. (b) Pavarini, E.; Yamanaki, A.; Nuss, J.; Andersen, O. K. *New J. Phys.* **2005**, *7*, 188.
(19) Yee, K. A.; Albright, T. A.; Jung, D.; Whangbo, M.-H. *Angew. Chem., Int. Ed. Engl*. **1989**, *28*, 750−751.
(20) (a) Whangbo, M.-H.; Ren, J.; Liang, W.; Canadell, E.; Pouget, J.-P.; Ravy, S.; Williams, J. M.; Beno, M. A. *Inorg. Chem*. **1992**, *31*, 4169−4173. (b) Rousseau, R.; Palacín, M. R.; Gómez-Romero, P.; Canadell, E. *Inorg. Chem*. **1996**, *35*, 1179−1184.
(21) Hase, I.; Nishihara, Y. *Phys. Rev. B* **1998**, *58*, 1707−1709.
(22) (a) Pickett, W. E.; Singh, D.; Papaconstantopoulos, D. A.; Krakauer, H.; Cyrot, M.; Cyrot-Lakmann, P. *Physica C* **1989**, *162*−*164*, 1433−1434. (b) Singh, D.; Papaconstantopoulos, D. A.; Krakauer, H.; Klein, B. M.; Pickett, W. E. *Physica C* **1991**, *175*, 329−334.
(23) (a) Kuntscher, C. A.; Gerhold, S.; Nücker, N.; Cummins, T. R.; Lu, D.-H.; Schuppler, S.; Gopinath, C. S.; Lichtenberg, F.; Mannhart, J.; Bohnen, K.-P. *Phys. Rev. B* **2000**, *61*, 1876−1883. (b) Winter, H.; Chuppler, S.; Kuntscher, C. A. *J. Phys.: Condens. Matter* **2000**, *12*, 1735−1751.
(24) (a) Hohenberg, P.; Kohn, W. *Phys. Rev*. **1964**, *136*, B864−B871. (b) Kohn, W.; Sham, L. J. *Phys. Rev*. **1965**, *140*, A1133−A1138.
(25) Soler, J. M.; Artacho, E.; Gale, J. D.; García, A.; Junquera, J.; Ordejón, P.; Sánchez-Portal, D. *J. Phys.: Condens. Matter*. **2002**, *14*, 2745−2779.
(26) http://www.uam.es/siesta/.
(27) For reviews on applications of the SIESTA approach, see: (a) Ordejón, P. *Phys. Status Solidi B* **2000**, *217*, 335−356. (b) Sánchez-Portal, D.; Ordejón, P.; Canadell, E. *Struct. Bonding* **2004**, *113*, 107−170.
(28) Perdew, J. P.; Burke, K.; Ernzerhof, M. *Phys. Rev. Lett.* **1996**, *77*, 3865−3688.
(29) Trouiller, N.; Martins, J. L. *Phys. Rev. B* **1991**, *43*, 1993−2006.
(30) Kleinman, L.; Bylander, D. M. *Phys. Rev. Lett.* **1982**, *48*, 1425−1428.

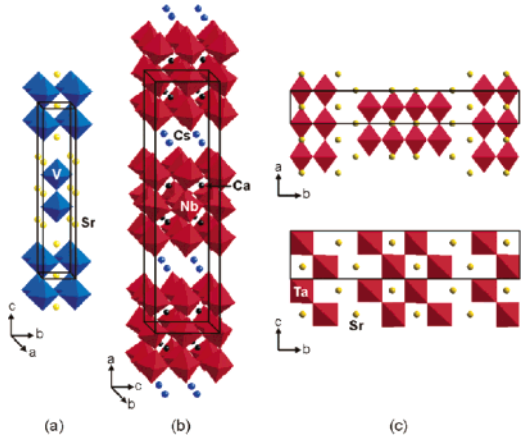

Figure 1. Crystal structure of (a) $Sr_3V_2O_7$, (b) $CsCa_2Nb_3O_{10}$, and (c) $Sr_2Ta_2O_7$ at room temperature.

in the core region were used for Sr, V, Nb, and Ta.[31] We have used a split-valence double-ζ basis set including polarization orbitals for all atoms, as obtained with an energy shift of 100 meV.[32] The energy cutoff of the real space integration mesh was 300 Ry. The Brillouin zone (BZ) was sampled using grids of (3 × 3 × 2) and (21 × 21 × 3) *k*-points[33] for determination of the density and Fermi surface, respectively. We have checked that the results are well converged with respect to the real space grid, the BZ sampling, and the range of the atomic orbitals. As a check for our approach, we first recalculated the electronic structure of $RbLaNb_2O_7$ using the same idealized structure employed by Hase and Nishihara in their FLAPW study.[21] Our calculations lead to similar results, the only difference resulting from the use of the f orbitals of La by these authors. This leads to the appearance of a set of flat bands at higher energies than those relevant here. The topology (shape and dispersion) of the lower-lying t_{2g}-block bands is not affected at all by the inclusion of the f orbitals and thus was not included in our work.

The semiempirical tight-binding band structure calculations were based upon the effective one-electron Hamiltonian of the extended Hückel method.[34] The off-diagonal matrix elements of the Hamiltonian were calculated according to the modified Wolfsberg−Helmholz formula.[35] Double-ζ Slater-type orbitals were used for transition metal d levels, but single-ζ Slater-type orbitals were used otherwise. The exponents and ionization potentials used were taken from a previous work.[36]

Results and Discussion

A. Crystal Structure. A MO_4 octahedral layer is formed upon corner sharing of all equatorial oxygen atoms of MO_6 octahedra. When these layers condense by sharing apical oxygens, they lead to M_nO_{3n+1} slabs, where *n* is the number of octahedral layers. These are the octahedral slabs present in the R−P and D−J phases. Shown in Figure 1 are the crystal structures of $Sr_3V_2O_7$[37] and $CsCa_2Nb_3O_{10}$.[38] The first is a double layer R−P phase, whereas the second is a triple layer D−J phase. The essential difference between the two families of phases lies in the cations location. Part of the cations are located in the holes inside the octahedral slabs, leading to $A_{n-1}B_nO_{3n+1}$ slabs in both cases. However, as the comparison of Figure 1a and b shows, the van der Waals gaps are less filled in the D−J ($A'[A_{n-1}B_nO_{3n+1}]$) than in the R−P ($A_2'[A_{n-1}B_nO_{3n+1}]$) families. The octahedral slabs of the different phases within a given family do not only differ in the number of octahedral layers but in the octahedral distortions, tiltings, etc. In the context of the present work, an especially relevant structural aspect that has strong consequences for the electronic structure is the difference between the two $M-O_{apical}$ distances of the octahedra. For instance, whereas the difference is small in $Sr_3Ti_2O_7$ (Δ = 0.013 Å)[39] or $Sr_3V_2O_7$ (Δ = 0.10 Å),[37] it can be as large as ∼0.6 Å in $KLaNb_2O_7$[40] or $LiLaTa_2O_7$.[41] This factor acquires especial relevance for $n > 2$. There the bond length difference tends to decrease for the inner layer(s), something that can be relevant when considering the electronic distribution within these slabs. To be able to thoroughly discuss the influence of the different structural aspects on the nature of the bottom t_{2g}-block bands of these systems, we have chosen to study a large set of these phases exhibiting a representative series of structural variations: R−P phases with double layers ($Sr_3V_2O_7$,[37] $Li_2SrNb_2O_7$,[42] $Rb_2LaNb_2O_7$[13]) and triple layers ($Ca_4Ti_3O_{10}$,[39] $K_2La_2Ti_3O_{10}$,[43] $Sr_4V_3O_{9.7}$[44]) as well as D−J phases with double layers ($KLaNb_2O_7$,[40] $RbLaNb_2O_7$[13]) and triple layers ($CsCa_2Nb_3O_{10}$[38]).

The topology of the octahedral condensation within the layers can also strongly affect the electronic structure, so to make our study as complete as possible we also have considered the above-mentioned series of $A_nB_nO_{3n+2}$ phases (see Figure 1c).[45] Their M_nO_{3n+2} slabs can be built from a M_nO_{5n+1} zigzag unit of *n* octahedra ($n = 4$ in **1**). These units lead to chains M_nO_{4n+2} (**2**) upon sharing $n - 1$ equatorial oxygen atoms and finally to the M_nO_{3n+2} layer (**3**) upon sharing all of their apical oxygen atoms. $Ln_2Ti_2O_7$,[46] $Sr_2Nb_2O_7$,[47] and $Ca_2Nb_2O_7$[48] are examples of this type of phase. $Sr_2Nb_2O_7$[47] and $Sr_2Ta_2O_7$[49] have been shown to exhibit a ferroelectric transition at 1342 and −107 °C, respectively, which is associated with severe distortions in the octahedra. For this family, we have considered both structures, before and after the transition, for $Sr_2Ta_2O_7$ ($n = 4$)[50] as well as the room-temperature structure of $Sr_2Nb_2O_7$ ($n = 4$), with even stronger octahedral distortions, to analyze

(31) Louis, S. G.; Froyen, S.; Cohen, M. L. *Phys. Rev. B* **1982**, *26*, 1738−1742.
(32) Artacho, E.; Sánchez-Portal, D.; Ordejón, P.; García, A.; Soler, J. M. *Phys. Status Solidi B* **1999**, *215*, 809−817.
(33) Monkhorst, H. J.; Park, J. D. *Phys. Rev. B* **1976**, *13*, 5188−5192.
(34) Whangbo, M.-H.; Hoffmann, R. *J. Am. Chem. Soc.* **1978**, *100*, 6093−6098.
(35) Ammeter, J. H.; Bürgi, H.-B.; Thibeault, J.; Hoffmann, R. *J. Am. Chem. Soc.* **1978**, *100*, 3686−3692.
(36) (a) Alemany, P.; Canadell, E. *Eur. J. Inorg. Chem.* **1999**, 1701−1706. (b) Doublet, M.-L.; Canadell, E.; Whangbo, M.-H. *J. Am. Chem. Soc.* **1994**, *116*, 2115−2120.
(37) Suzuki, N.; Noritake, T.; Yamamoto, N.; Hioki, T. *Mater. Res. Bull.* **1991**, *26*, 1−9.
(38) Dion, M.; Ganne, M.; Tournoux, M.; Ravez, J. *Rev. Chim. Miner.* **1984**, *21*, 92−103.
(39) Elcombe, M. M.; Kisi, E. H.; Hawkins, K. D.; White, T. J.; Goodman, P.; Matheson, S. *Acta Crystallogr.* **1991**, *47*, 305−314.
(40) Sato, M.; Abo, J.; Jin, T.; Ohta, M. *J. Alloys Compd.* **1993**, *192*, 81−83.
(41) Toda, K.; Sato, M. *J. Mater. Chem.* **1996**, *6*, 1067−1071.
(42) Floros, N.; Michel, C.; Hervieu, M.; Raveau, B. *J. Mater. Chem.* **1999**, *9*, 3101−3106.
(43) Toda, K.; Watanabe, J.; Sato, M. *Mater. Res. Bull.* **1996**, *31*, 1427−1435.
(44) Gong, W. H.; Xue, J. S.; Greedan, J. E. *J. Solid State Chem.* **1991**, *91*, 180−185.
(45) Lichtenberg, F.; Herrnberger, A.; Wiedenmann, K.; Mannhart, J. *Prog. Solid State Chem.* **2001**, *29*, 1−70.
(46) (a) Scheunemann, K.; Müller-Buschbaum, H. K. *J. Inorg. Nucl. Chem.* **1975**, *37*, 1879−1881. (b) Gasperin, M. *Acta Crystallogr., Sect. B* **1975**, *31*, 2129−2130. (c) Tanaka, M.; Sekii, H.; Ohi, K. *Jpn. J. Appl. Phys.* **1985**, *24*, 814−816. (d) Williams, T.; Lichtenberg, F.; Widmer, D.; Bednorz, J. G.; Reller, A. *J. Solid State Chem.* **1993**, *103*, 375−386.
(47) Ishizawa, N.; Marumo, F.; Iwai, S.; Kimura, M.; Kawamura, T. *Acta Crystallogr., Sect. B* **1975**, *31*, 1912−1915.
(48) Ishizawa, N.; Marumo, F.; Iwai, S.; Kimura, M.; Kawamura, T. *Acta Crystallogr., Sect. B* **1980**, *36*, 763−766.
(49) (a) Ishizawa, N.; Marumo, F.; Iwai, S.; Kimura, M.; Kawamura, T. *Acta Crystallogr., Sect. B* **1976**, *32*, 2564−2566. (b) Ishizawa, N.; Marumo, F.; Iwai, S. *Acta Crystallogr., Sect. B* **1981**, *37*, 26−31.
(50) Although according to the general formula the $n = 4$ phases should be referred to as $A_4B_4O_{14}$, both $A_2B_2O_7$ and $ABO_{3.5}$ are more commonly used in the literature and will also be used here.

the effect of the transition metal and these distortions on the nature of the bottom t_{2g}-block bands of this type of phase.

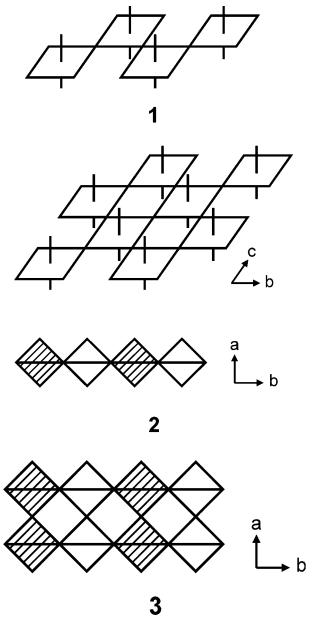

B. Qualitative Model for Single and Double Layer Systems. As mentioned, we will consider systems where only the bottom part of the t_{2g}-block bands is filled, that is, with d^x ($0 \le x \le 1$) transition metal atoms. To elaborate a simple model able to highlight the correlation between the crystal structure details and the nature of the partially filled bands (and thus the Fermi surface) of these materials, it is useful to consider the case of an ideal single MO_4 octahedral layer with all M−O distances identical and angles equal to 90° and 180°. Later, we will consider the effect of layer condensation to lead to double layers, triple layers, etc., as well as different octahedral distortions present in the real layers. The unit cell directions and coordinate axis used in this section are defined in **4**.

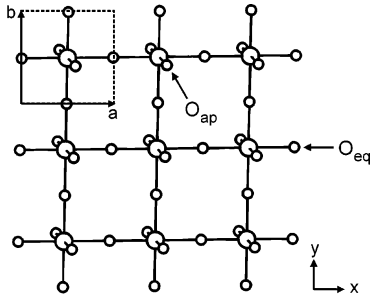

The t_{2g}-block band levels of a perovskite-type slab are raised in energy when the orbitals of the bridging oxygen atoms are allowed by symmetry to mix with the metal t_{2g} orbitals. Because there are no direct metal−metal interactions, this is the only feature to take into account when drawing a qualitative t_{2g}-block band structure for these materials, something that thus turns out to be extremely simple.[20b] Essentially, what we need to do to guess the energy dispersion and relative position of the different t_{2g}-block bands is just to count how many oxygen p orbital contributions can be found in the crystal orbitals of each band for different points of the BZ and draw a qualitative band

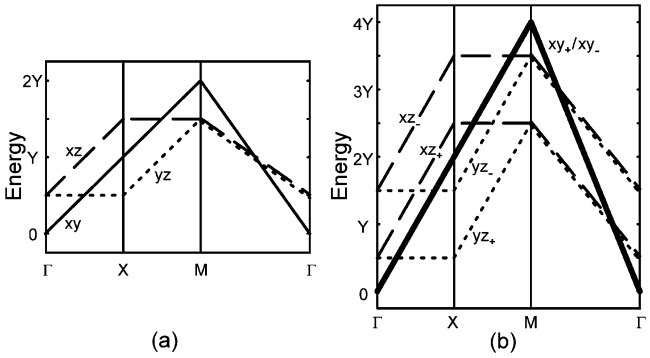

Figure 2. Qualitative band structures for an ideal (a) MO_4 single layer and (b) M_2O_7 double layer. The Γ, *X*, and *M* labels refer to the (0, 0), ($a^*/2$, 0), and ($a^*/2$, $a^*/2$) wave vectors, respectively.

structure on the basis of these results. This simple approach has been shown to be extremely helpful in understanding the nature of the partially filled bands of quite complex perovskite related materials.[51] The crystal orbitals for the *xy*, *xz*, and *yz* orbitals at Γ, *X*, and *M* are shown in **5a**−**c**, **6a**−**c**, and **7a**−**c**, respectively, where we have used dots to indicate the absence of oxygen p orbitals in the bridging equatorial positions (O_{eq} in **4**) for these crystal orbitals. To draw a qualitative band structure, we need to consider also the role of the apical oxygen atoms (O_{ap} in **4**). For simplicity, these contributions have not been shown in **5**−**7**, but it is easy to see that there are two apical contributions per transition metal atom in **6a**−**c** and **7a**−**c** but none for **5a**−**c**.

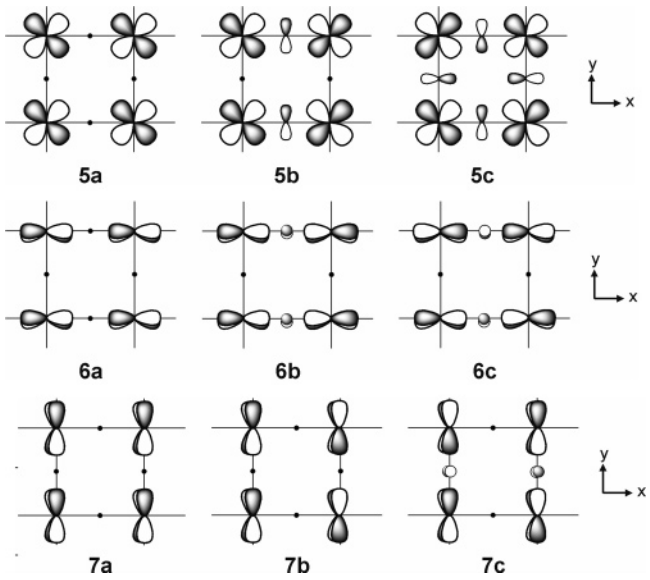

Thus, the total number of oxygen antibonding contributions per repeat unit of the layer to the *xy*, *xz*, and *yz* bands for selected points of the BZ can be easily counted.[20b] Taking into account that the energy destabilization due to an oxygen p orbital in a bridging equatorial position (*Y*) and that at a terminal apical position (*y*) are related by the relationship $Y \approx 4y$,[51] the qualitative band structure for the ideal MO_4 single layer can be drawn[20b] (see Figure 2a; note that the bands in this and the following schematic band diagrams are drawn as straight lines for simplicity). Essentially, the t_{2g}-block band structure is the

(51) Canadell, E.; Whangbo, M.-H. *Chem. Rev.* **1991**, *91*, 965−1034.

superposition of a two-dimensional (2D) band originating from the *xy* orbital and two one-dimensional (1D) bands originating from the *xz* and *yz* orbitals. The two 1D bands are dispersive along orthogonal directions; that is, the *xz* band is dispersive along *x* but flat along *y*, whereas the *yz* band is flat along *x* but dispersive along *y*. The lowest part of the band structure is associated with the *xy* band. However, the difference in energy between the bottom of the 2D and 1D bands is not large so that for most electron counts the two types of bands may well be partially filled. Taking into account the local orthogonality of the three t_{2g} orbitals, this means that the Fermi surface (FS) of this layer will result from the weak hybridization of a 2D and two orthogonal 1D FSs (for a detailed discussion on the dimensionality of the Fermi surface, see ref 51).

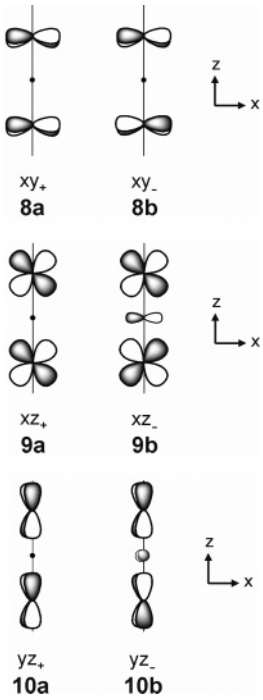

It is now easy to guess which will be the band structure of an ideal M_2O_7 double layer obtained by condensation of two MO_4 single layers. There are now two transition metal atoms per repeat unit and thus six t_{2g}-block bands. The orbitals of the $M-O_{ap}-M$ linkage leading to these six bands are schematically shown in **8a**,**b**, **9a**,**b**, and **10a**,**b** (again, we do not show for simplicity the contributions of the nonbridging O_{ap} contributions). There is an essential difference between the *xy* and *xz*/*yz* based combinations. Whereas no p orbital of the bridging apical oxygen can mix into the xy_+/xy_- combinations so that both are practically degenerate, one of the two *xz* and *yz* combinations can interact with a p orbital of the apical bridging oxygen atom, leading to a clear energy difference among them. The simple rule derived from this observation is that the number of oxygen p orbital contributions per repeat unit of the ideal M_2O_7 double layer is: (a) twice those of the single layer for both *xy* bands, (b) twice those of the single layer minus the two apical contributions ($2y = Y/2$) associated with the shared oxygen for the xz_+ and yz_+ bands, and (c) twice those of the single layer minus the two apical contributions of the shared position ($2y = Y/2$) plus the new bridging contribution (Y) for the xz_- and yz_- bands. The qualitative band structure for the ideal double-layer constructed on the basis of this rule is shown in Figure 2b.

Again, although the bottom of the two 2D bands (xy_+/xy_-) is the lowest part of the t_{2g}-block bands, the two 1D bands, xz_+ and yz_+, overlap with them for most electron counts. Consequently, for most metal electron counts the FS of the system will arise from the hybridization of two 2D FSs and two 1D FSs. As far as the octahedral distortions are weak so that the ideal layer is a good approximation to the real layer, the local orthogonality of the three t_{2g} orbitals will lead to a weak interaction of the 1D and 2D FSs and the real FS will practically be the superposition of the four contributions. In principle, these systems could then exhibit the kind of charge and/or spin density wave (CDW/SDW) instabilities arising at low temperatures for 1D or pseudo-1D metals and destroying an important fraction of the FS, thus leading to anomalies in the resistivity versus temperature curves.[51] However, if the octahedral distortions are such that the xz_+ and yz_+ bands are raised in energy so that for the electron counts considered here they are not partially filled, only the 2D bands will contribute to the FS and the systems will be immune to such electronic instabilities and the physical behavior will be distinctly different. With the qualitative analysis proposed above, it is simple to guess (or rationalize) how different octahedral distortions can affect the nature of the bottom t_{2g}-block bands. For instance, the separation between the bottom of the xy_+/xy_- and xz_+/yz_+ bands is due to the two p orbital contributions of the nonbridging O_{ap} atoms. Thus, the bottom of the xz_+/yz_+ bands will be raised in energy if the $M-O_{apical}$ distances are shorter than the average M−O bond length. This kind of distortion is frequently encountered in these materials where the outer $M-O_{apical}$ distance is usually shorter than the inner one although to a different degree depending on the materials. Thus, this structural feature is expected to play an important role in determining the physical behavior of these materials.

As a test of our simple model, we have calculated the extended Hückel band structure for a Ta_2O_7 double-layer with ideal octahedra (Figure S1a) and with $M-O_{apical}$ distances differing by 0.6 Å (Figure S1b), as found in several D−J and R−P phases. The agreement between the calculated band structure for the nondistorted case (Figure S1a) and that of Figure 2b is excellent, and comparison between the calculated band structures for the nondistorted and distorted cases (Figures S1a and S1b, respectively) shows that the predicted trend is indeed observed. Thus, we conclude that the simple model provides a useful tool in understanding the gross features of the bottom t_{2g}-block bands of these phases. To have a more quantitative measure of how the different structural departures from ideality affect the key aspects in discussing the nature of the FS of these materials, that is, the extent of hybridization among the 1D and 2D contributions to the FS and the separation between the 2D and 1D bands, in the next section we report first-principles calculations for several of these materials.

C. First-Principles Results for Double Layer Systems. We discuss here the electronic structure of a series of double layer systems, $KLaNb_2O_7$,[40] $Li_2SrNb_2O_7$,[42] $Rb_2LaNb_2O_7$,[13] and $Sr_3V_2O_7$[37] (Figure 1a), which we have chosen because (a) the transition metal is in a d^0 configuration for the first two phases whereas it is in a $d^{0.5}$ and d^1 for the third and fourth, respectively; (b) the difference between the two $M-O_{apical}$ distances decreases

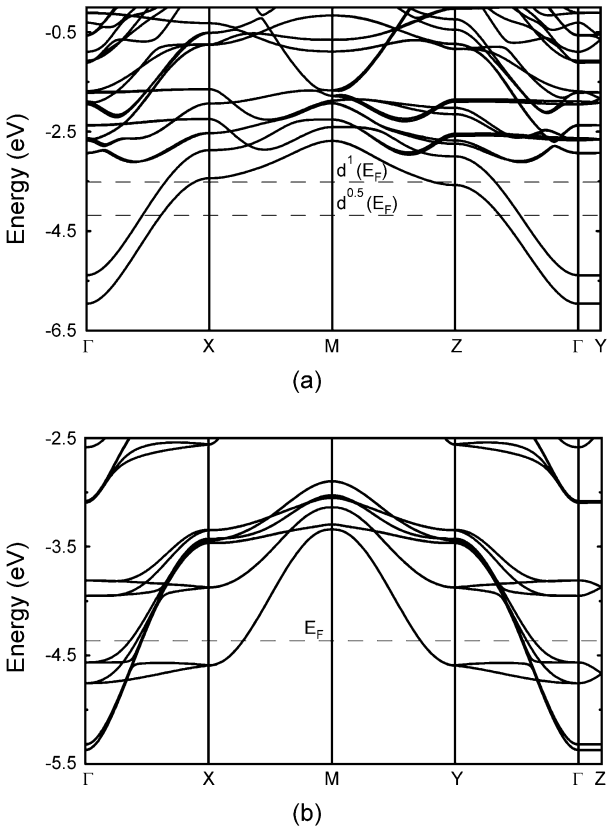

Figure 3. First-principles band structures for $KLaNb_2O_7$ (a) and $Sr_3V_2O_7$ (b). The dashed lines in (a) refer to the Fermi levels calculated assuming a rigid band scheme for the situations in which the Nb atoms are formally in $d^{0.5}$ and d^1 configurations. The dashed line in (b) refers to the real Fermi level. The Γ, *X*, *Y*, *Z*, and *M* labels refer to the (0, 0, 0), (*a**/2, 0, 0), (0, *b**/0, 0), (0, 0, *c**/2), and (*a**/2, *b**/2, 0) wave vectors, respectively.

from 0.56 Å in $KLaNb_2O_7$[40] to 0.10 Å in $Sr_3V_2O_7$;[37] (c) the tilting of the octahedra is important in the second and third phases but nil in the first and fourth; and (d) the last three phases are R−P phases, whereas the first one is a D−J phase. Thus, we can test how the more relevant structural and electronic features of the double layer systems influence the nature of the partially filled t_{2g} bands and the FS while considering systems mostly of interest by themselves.

As mentioned, $KLaNb_2O_7$ exhibits metallic behavior under lithium intercalation.[10a] The two Nb−O_{apical} distances in the nonintercalated phase are 1.695 and 2.255 Å, and there is no tilting of the octahedra.[40] Thus, we are in the ideal situation for having the 1D bands well above the 2D bands. The calculated band structure is shown in Figure 3a where the two lower bands (in fact, every one of these bands is really a pair of bands because there are two double layers per unit cell and the interaction along the interlayer direction is nil) are the xy_+ and xy_- ones. Assuming a rigid band scheme, these bands are those that would be filled for electron fillings as large as those associated with metal atoms in a d^1 configuration. The calculated FS for the $d^{0.5}$ case is shown in Figure 4a. As shown in Figure 3a, the band dispersion along the *b*-direction (i.e., the interlayer direction; see Γ→*Y* in Figure 3a) is nil. This is a general result for all phases studied as far as the *xy* bands are concerned, which is easily understood. Because of the δ-type interactions along the M−O_{apical} bond, the outer oxygen atoms do not contribute to these bands, and this practically cuts all interactions along the interlayer direction. Thus, we just show one section of the

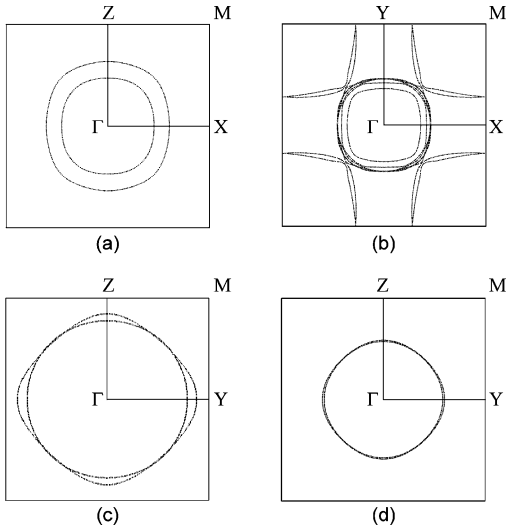

Figure 4. First-principles FSs calculated for (a) $KLaNb_2O_7$ for a band filling corresponding to $d^{0.5}$ Nb atoms (section $k_y = 0$); (b) $Sr_3V_2O_7$ (section $k_z = 0$); (c) $Rb_2LaNb_2O_7$ (section $k_x = 0$); and (d) $Li_2SrNb_2O_7$ for a band filling corresponding to $d^{0.25}$ Nb atoms (section $k_x = 0$).

FS perpendicular to the interlayer direction. As predicted by the simple scheme, this section contains two pairs of closed circular loops so that the FS is a series of four cylinders. Because this is the case for any band filling corresponding to Nb atoms between d^0 and d^1 and the reported intercalation experiments suggest band filling values (see below) certainly lower than those associated with a d^1 situation, we conclude that $Li_xKLaNb_2O_7$ must be a 2D metal. Consequently, it should be a stable metal immune to the low-temperature resistivity anomalies usually associated with 1D systems. The structures of the different $ALaNb_2O_7$ phases[13,40] are practically identical, the main difference being the change in the *b* parameter as a consequence of the different size of the A cation. Because the interlayer interactions are nil (and the separation will further increase under intercalation), all phases of this series should be 2D metals under intercalation. The only difference from the qualitative scheme lies in the fact that there is a slight splitting between the xy_+ and xy_- bands. This means that even if the partially filled levels are mainly based on the *xy* levels there is some coupling between the two layers of the double layer. This is so because of the inclusion of d-levels in the basis set used for the oxygen atoms, a feature absent in the simple model. However, let us note that among all compounds studied this is the one in which this interaction seems to be the largest (this fact seems to be only relevant when the difference between the two Nb−O_{apical} distances is large).

In $Sr_3V_2O_7$, the difference between the two Nb−O_{apical} distances is small (1.87 and 1.97 Å),[37] there is no tilting of the octahedra (i.e., the double layer is close to ideal, see Figure 1a), and the metal configuration is d^1. These are the ideal conditions to have 1D bands partially filled. The calculated band structure for this material is shown in Figure 3b. The 2D bands are really the superposition of a pair of bands because again the interlayer interactions are nil (see the Γ→*Z* direction in Figure 3b). The pairs of 1D bands are slightly split because of the occurrence of weak interlayer interactions (see the Γ→*Z* direction in Figure 3b). The agreement with the qualitative band structure is striking and fully confirms our approach. The weak interplanar coupling associated with the 1D bands arises because

the apical oxygen p orbitals mix into the *xz* and *yz* based bands. However, as it is clear from the band structure and the small warping of the calculated FSs of $Sr_3V_2O_7$, the interlayer interaction is weak. Consequently, independent of the nature of the partially filled bands, the interlayer coupling is practically negligible as far as these bands are concerned, and the simple model is equally applicable to the R−P and D−J phases. A section of the calculated FS is shown in Figure 4b. It is simply the superposition of two pairs of circular loops and four pairs of slightly warped lines along orthogonal directions. Thus, the real 3D FS results from the superposition of two pairs of cylinders (one pair per double layer), two pairs of slightly warped planes perpendicular to the *a*-direction, and two pairs of slightly warped planes perpendicular to the *b*-direction. As expected from the simple model, the conductivity of this system should be 2D but not because of the existence of genuine 2D bands only. The superposition of two orthogonal 1D systems associated with the *xz* and *yz* orbitals to the genuine 2D system associated with the *xy* orbitals confers nesting properties to the FS, and thus the possibility of structural modulations and the associated resistivity anomalies at low temperature arises.[20] Careful transport studies on single crystals of this phase would be most interesting.

The transition metal atoms in $Rb_2LaNb_2O_7$ are formally $d^{0.5}$, and consequently the lower t_{2g} bands must be partially filled. The two $Nb-O_{apical}$ distances are 1.842 and 2.110 Å, and the octahedra are tilted[13] so that the repeat unit of the double layer contains now four octahedra instead of just two as for the previous cases. A section of the calculated FS is shown in Figure 4c. The two closed loops (really two pairs of closed loops) are now similar because the interaction between the two layers of the double layer is weak. Clearly, the smaller apical bond length difference and the tilting of the octahedra do not appreciably change the situation with respect to the case of $KLaNb_2O_7$. The only difference is that the 1D bands start to play a role for lower electron fillings. In fact, $Rb_2LaNb_2O_7$ is an interesting system for several reasons. First, the transport properties of this phase have not been investigated. Thus, it would be interesting to confirm the predicted metallic behavior and, if the answer is positive, to see if it becomes superconducting at low temperature. Because this system is free from the disorder problems associated with intercalated layered materials, it may be a useful test of the idea that the intercalated double layer materials do not become superconducting, in contrast with the triple layer ones, because of the disorder in the interlayer region, which affects the whole double layer but not the central layer in the triple layer phases. Second, partial cation substitution in this material may be a way to make the 1D bands become partially filled and thus change the transport properties even if the difference in $Nb-O_{apical}$ distances is not that small.

Finally, in $Li_2SrNb_2O_7$ the difference between the two $Nb-O_{apical}$ distances is smaller (1.864 and 2.082 Å) and the octahedra are also tilted.[42] The calculated FS for a $d^{0.25}$ situation is shown in Figure 4d, and again it is clear that only the 2D bands should play a role in the conductivity for this filling. As expected from the simple model, the 1D bands would start to play a role for lower fillings of the bands. In fact, now they already start to be filled for electron fillings corresponding to Nb in a $d^{0.5}$ configuration. From all of the compounds we have studied, it is quite clear that even for small differences in the $Nb-O_{apical}$ distances and independently of the fact that the octahedra are tilted or not, for electron fillings lower than those corresponding to a $\sim d^{0.45}$ formal configuration of the metal, only the 2D bands should be partially filled. Although it is difficult to guess how effective will be the intercalation process in filling the t_{2g} bands, the data of Fukuoka et al.[10c] for the triple layer compound $Li_xKCa_2Nb_3O_{10}$ may be taken as suggestive that a $d^{0.4}$ situation would not be unreasonable. If this is correct, our analysis suggests that for most intercalated double layer phases with transition metals originally in a d^0 configuration, the conductivity should be 2D and thus be stable metals until low temperatures. Further studies on these materials would be helpful in understanding the possible occurrence of superconductivity.

D. Qualitative Model for Triple Layer Systems. Extension of the simple model to an M_3O_{10} triple layer is straightforward. We only need to consider how the fact of having two different types of octahedral layers influences the results. As far as the *xy* orbitals are concerned, the situation has not changed. Because they make δ-type interactions along the apical axis, we merely have three identical 2D bands identical in nature to those of the single layer. For the *xz*/*yz* orbitals, the situation is also easily understood. The three possible combinations for the *xz* orbitals are shown in **11a**−**c**. For **11a**, the number of oxygen p orbital contributions per repeat unit of the ideal M_3O_{10} triple layer is 3 times that of the single layer minus four apical contributions ($4y = Y$) associated with the shared oxygen positions. For **11c**, we simply need to add to the previous count the contribution of the two interlayers shared positions ($2Y$), which now are engaged in antibonding interactions with the *xz* orbitals. For **11b**, one must be careful because of the normalization effect on the orbital coefficients (here, there are no metal contributions in one of the layers), but it is easy to see that the band must be always equidistant of the two previous ones. Thus, the simple qualitative band structure shown in **12** can be drawn.

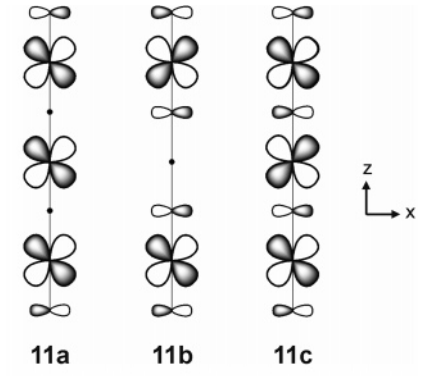

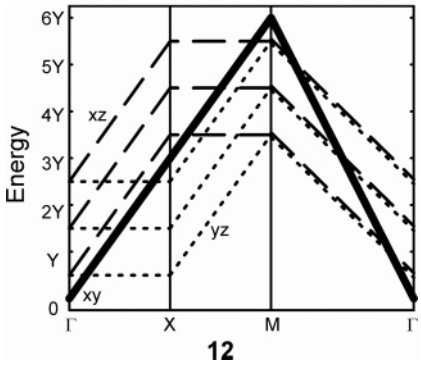

On the basis of the qualitative diagrams, the double and triple layer systems differ in two aspects. First, there is a decrease of the separation between the bottom part of the 1D and 2D bands; this favors the coexistence of closed and open features in the FS for lower t_{2g}-block band fillings. Second, the existence of two types of octahedral layers makes different the participation of each type of layer in the bands. It is clear that the inner layer octahedra will be in general more regular than those of the outer layers. If the difference is sizable, some of the lower bands will tend to be localized in the central layer and, consequently, an important fraction of the electrons will mostly reside in this inner octahedral layer. This is an important feature that can have strong implications for the transport properties of these systems. For instance, it has been proposed[10a] that the fact that superconductivity has been induced by intercalation in triple layer systems but not in double layer ones is related to a preferential occupation of the inner layer sites by the transferred electrons. To test how much the apical octahedral distortions typically found in these systems can affect the topology of the "ideal" band structure, we have calculated the extended Hückel band structure for an ideal and distorted Ta_3O_{10} triple layer (see Figure S2). Here, the distortion affects only the two apical octahedral bond lengths of the outer layers, which were changed by ± 0.3 Å with respect to the ideal ones. The band structure for the ideal system completely agrees with our simple model, and the outer layers octahedral distortion clearly modifies this band structure by leaving the *xy* bands unaltered but considerably affecting the *xz*/*yz* bands. The lower pair of bands of this type lies now higher in energy and is mostly concentrated in the inner layer (80% for the model calculation of Figure S2b), whereas the two upper lying pairs of bands concentrate in the outer layers.

In summary, for triple layers the 1D bands start to play a role for lower d electron counts than they do for the double layer systems as far as there are no sizable octahedral apical distortions in the outer layers. In addition, the 1D electrons tend to concentrate on the inner layer when these distortions occur. However, the 2D electrons are almost equally distributed among the three layers.

E. First-Principles Results for Triple Layer Phases. Calculations have been carried out for several phases including $Ca_4Ti_3O_{10}$,[39] $K_2La_2Ti_3O_{10}$,[43] $CsCa_2Nb_3O_{10}$[38] (Figure 1b), and $Sr_4V_3O_{9.7}$.[44] The first three phases are d^0 compounds, and the third is one of the members of the series of triple layer compounds that after lithium intercalation become superconducting. The last one is nearly d^1 and is metallic. The first two systems contain the same transition metal, but whereas the octahedra are tilted in the first one, they are not in the second. In addition, the difference between the two outer layer $Ti-O_{apical}$ distances is small (1.905 and 1.981 Å) in the first but large in the second (1.718 and 2.296 Å).

In terms of the difference between the two outer layer $Ti-O_{apical}$ distances, $Ca_4Ti_3O_{10}$ is the most regular of the triple layer compounds we have considered. The octahedra are tilted, but, except for the fact that the number of octahedra in the repeat unit doubles, this has no major consequence for the electronic structure, as it was found for the double layer materials. According to the qualitative scheme, the 1D bands should start to play a role for lower electron fillings than they do for the double layer compounds. This expectation is in complete agreement with the results for this system. Shown in Figure 5a and b are sections of the FS calculated for the case where the metal atoms would formally be in $d^{0.1}$ and $d^{0.5}$ configurations, respectively. In the first case, there are three pairs of circular loops (the larger circle is in fact the superposition of four circles) with a weak separation. This is what is expected for a triple layer system with a low electron filling of the bands and where the interaction between the *xy*-type bands of the different layers of the triple layer is small. In the second case (in which we use a repeated zone representation), 1D components along orthogonal directions[52] are superposed to the 2D ones. In fact, the 1D bands begin to be filled for band fillings as low as those corresponding to $d^{0.16}$.

As noted above, in $K_2La_2Ti_3O_{10}$ there is a large difference between the two outer layer $Ti-O_{apical}$ distances. This has a major effect on the calculated band structure and FS. The 1D bands are strongly raised in energy in such a way that only for an electron filling corresponding to a formal $d^{0.5}$ configuration of the metal do they start to be occupied. These observations completely substantiate the simple scheme. The presently available results[10,11] suggest that the band fillings attainable for triple layer systems under lithiation should probably be lower than those corresponding to $d^{0.26}$. Thus, as far as the two outer $M-O_{apical}$ distances are not similar, it is likely that the FS of these systems will be purely 2D. In contrast, we note that the triple layer compound $Sr_4V_3O_{9.7}$ exhibits a regular structure with outer layer $V-O_{apical}$ distances of 1.951 and 1.988 Å. This feature and the relatively large band filling (d^1 V atoms) lead to a different FS, that is, of the same type as that of Figure 5b, in which the 1D bands play an important role.

The $AB_2Nb_3O_{10}$ phases (A = alkaline metal; B = alkaline-earth metal) are those that have been more thoroughly considered in lithium intercalation studies, and most of them have been found to be metallic and superconducting.[10,11] The original nonlithiated phases of this family exhibit an important difference ($\sim 0.5-0.6$ Å) in the $Nb-O_{apical}$ distances of the outer layer octahedra. Thus, the lithiated systems are expected to be 2D metals. Here, we report on one of the phases of this series, $CsCa_2Nb_3O_{10}$. The calculated FSs for $d^{1/3}$ and $d^{0.5}$ formal Nb configurations are shown in Figure 6. That of Figure 6a, which should be close to the FS of the lithiated phase, is made of three pairs of circular loops (the inner one is really the superposition of four circles, whereas the outer one is the superposition of two). This is again close to the prediction of the simple scheme. When the filling of the band increases, the area of the circles increases and the actual section looks more complicated, but still they result from the hybridization of six circles (see Figure 6b). It is clear that for the real lithium contents observed up to now for these phases and even clearly larger, the real FS is made of a series of cylinders, and thus these lithiated phases are purely 2D metals. An important result of Figure 6a is that the three pairs of circles almost superpose. This means that, in agreement with the simple model, the *xy* based bands of the three layers in the triple layer are practically degenerate, and, consequently, the transferred electrons are almost equally distributed among the three layers. We have

(52) Note that because of the tilting of the octahedra the unit cell doubles and the new repeat vectors are rotated by 45° with respect to those of the reference unit cell. As a consequence, the 1D components of the FS in Figure 5b are also rotated 45° with respect to those of Figure 4b.

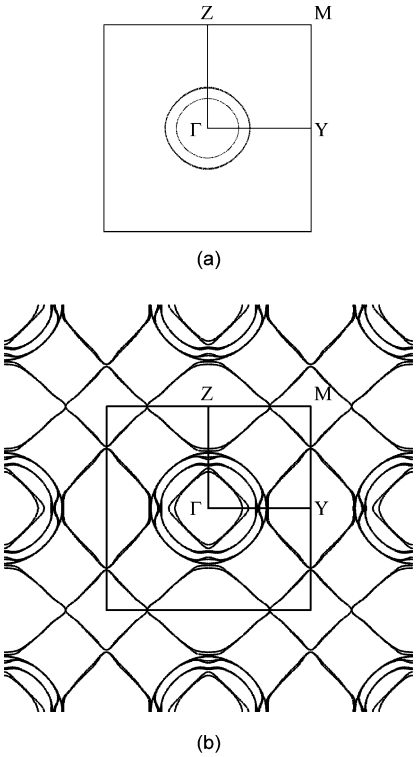

Figure 5. First-principles FS calculated for $Ca_4Ti_3O_{10}$ (section $k_x = 0$) assuming a band filling corresponding to $d^{0.1}$ (a) and $d^{0.5}$ (b). For (b), we use a repeated zone representation.

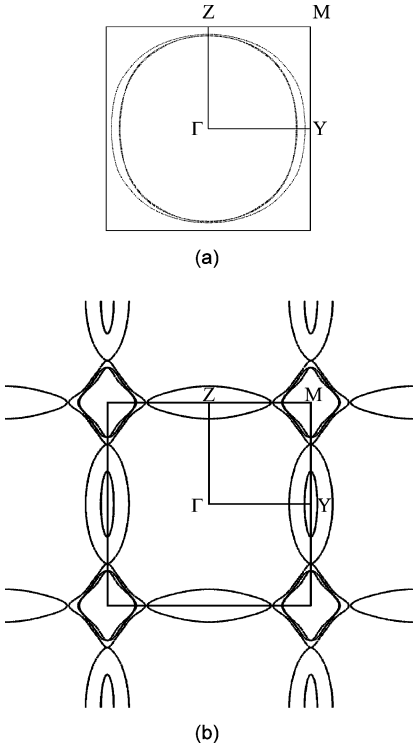

Figure 6. First-principles FS calculated for $CsCa_2Nb_3O_{10}$ (section $k_x = 0$) assuming a band filling corresponding to $d^{1/3}$ (a) and $d^{0.5}$ (b). For (b), we use a repeated zone representation.

verified this by evaluating the actual electron distribution for different band fillings.

These results do not seem to agree with previous suggestions concerning the appearance of superconductivity in $Li_xKCa_2Nb_3O_{10}$ but not in $Li_xKLaNb_2O_7$,[10a] according to which superconductivity arises because electrons tend to concentrate in the central layer and thus are immune to the influence of the disorder in the van der Waals gap. According to our results, there should not be accumulation of electrons in the central layer and the nature of the FS of the lithiated double layer and triple layer phases is identical. Later studies[11] have shown that $Li_xACa_2Nb_3O_{10}$ (A = Rb, K, Cs) and $Li_xASr_2Nb_3O_{10}$ (A = Rb, Cs) become superconducting but neither $Li_xCsBa_2Nb_3O_{10}$ nor the quadruple layer lithiated phase $Li_xKCa_2NaNb_4O_{13}$ do. The nature of the FS for the quadruple layer compound is again identical to those of the double and triple layer compounds, and the electrons at the Fermi level are equally distributed among the four layers. Thus, the screening by the outer layers cannot be the reason for the appearance of superconductivity in the triple layer compounds. Another factor to consider is the density of states at the Fermi level, $N(E_f)$. For a given host compound, the T_c values practically do not change once a threshold value of x is reached (for instance, $x = 0.1$ for $Li_xCsSr_2Nb_3O_{10}$), and typically values up to $\sim$0.75 are attainable. Because, as we have verified for $CsCa_2Nb_3O_{10}$, $N(E_f)$ changes appreciably in the corresponding range of band fillings, we believe that it cannot play a leading role in determining the T_c or the appearance of superconductivity. In our opinion, the driving force for the possible appearance of superconductivity and the actual T_c must be found in the lattice vibrations, which must strongly depend on the layer thickness and the nature of the cations. Clearly, more work in both double and quadruple layer lithiated materials is needed. It would also be interesting to test the possible appearance of superconductivity in the triple layer phase $Sr_4V_3O_{9.7}$ at temperatures lower than 4.2 K.

F. Qualitative Model for Quadruple Layer Systems of the $A_nB_nO_{3n+2}$ Phases. Extension of the simple model to a M_4O_{13} quadruple layer of the D−J or R−P series is obvious. Of more interest is to consider the M_4O_{14} quadruple layers present in the $n = 4$ members of the $A_nB_nO_{3n+2}$ family of phases[46] (see Figure 1c). Two members of this series, $Sr_{1-y}La_yNbO_{3.5-x}$ ($n = 4$) and $SrNbO_{3.41}$ ($n = 5$), have recently been the object of much attention because of their interesting transport properties.[23a,53] As discussed before, the layers of these compounds result from the condensation along the *a*- and *c*-directions of zigzag octahedral units, for instance, the quadruple unit **1** for the compound with $n = 4$. There are now four transition metal atoms per repeat unit and thus 12 t_{2g}-block bands. Here, again, we must count how many oxygen p antibonding contributions can occur for the 12 t_{2g}-block bands, that is, the x^2-y^2, *xz*, and *yz* based bands with the system of axis chosen (**13**). To do this as simply as possible, we must realize that there are four different types of such antibonding contributions, which, as shown in **13**, we will refer to as shared (O_{sh}), apical (O_{ap}), inner (O_{in}), and outer (O_{out}).

The two lower energy combinations of the x^2-y^2 orbitals (i.e., those with less oxygen p contributions) at Γ are shown in **14a** and **14b**. In both cases, there are four contributions of the O_{out} and no contribution from the O_{ap}. The difference between the two crystal orbitals lies in the appearance of one O_{in} and one

(53) (a) Weber, J.-E.; Kegler, C.; Büttgen, N.; Krug von Nida, H.-A.; Loidl, A.; Lichtenberg, F. *Phys. Rev. B* **2001**, *64*, 235414. (b) Kuntscher, C. A.; Schuppler, S.; Haas, P.; Gorshunov, B.; Dressel, M.; Grioni, M.; Lichtenberg, F.; Herrnberger, A.; Mayr, F.; Mannhart, J. *Phys. Rev. Lett.* **2002**, *89*, 236403. (c) Kuntscher, C. A.; Schuppler, S.; Haas, P.; Gorshunov, B.; Dressel, M.; Lichtenberg, F. *Phys. Rev. B* **2004**, *70*, 245123.

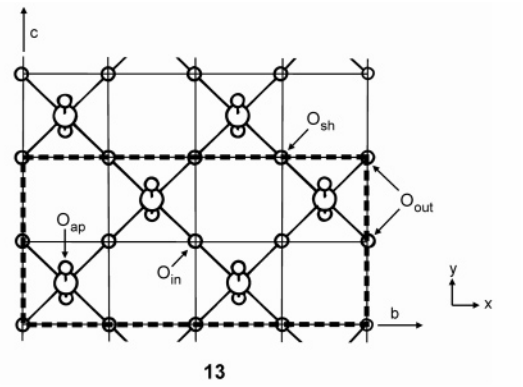

13

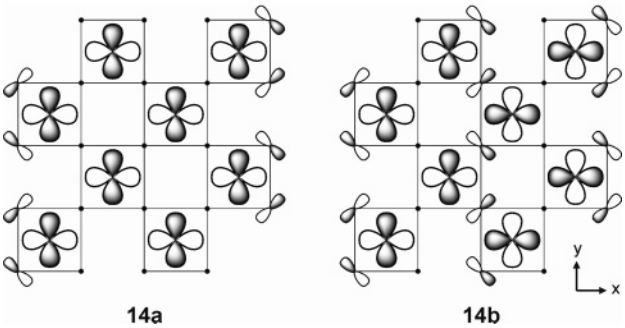

14a **14b**

O_{sh} contribution in **14b**. It is easy to see that the energy difference between the two crystal orbitals ($2Y$) is exactly the same for any two successive x^2-y^2 levels at Γ. Going from Γ to X, no additional antibonding contributions develop because of the δ-type interaction of the metal x^2-y^2 orbitals with the p orbitals of the apical oxygens. Taking into account the symmetry of the system, the four crystal orbitals are equivalent, and thus degenerate, at the Z point. Two of these combinations are shown in **15a** and **15b**. Now there are eight O_{out} contributions, that is, $8y = 2Y$, but because only one-half of the octahedra contribute to each crystal orbital, normalization doubles the weight of the antibonding contribution, and consequently the correct, effective, count is $4Y$.

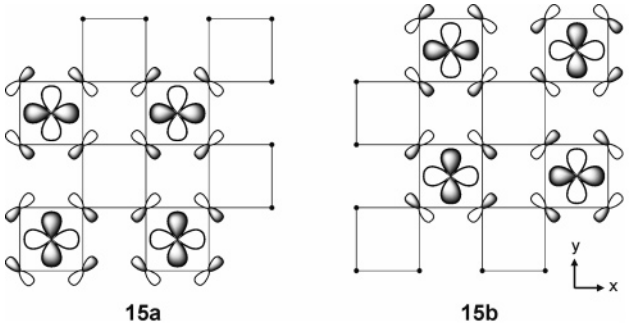

15a **15b**

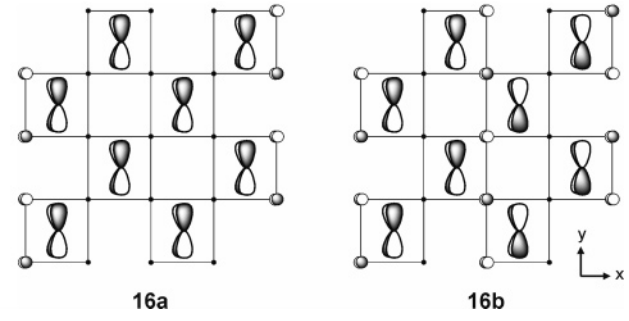

16a **16b**

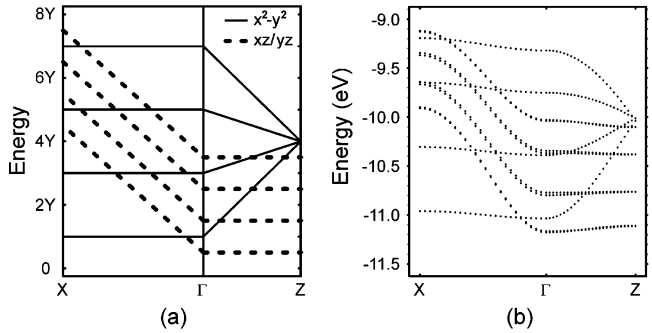

Figure 7. Band structure for the M_4O_{14} quadruple layers of the $A_nB_nO_{3n+2}$ ($n = 4$) phases: (a) qualitative band structure; and (b) calculated extended Hückel band structure for a Ta_4O_{14} layer with regular octahedra, that is, all Ta−O distances identical (1.95 Å) and angles of 90° and 180°. The Γ, X, and Z labels refer to the (0, 0), ($a^*/2$, 0), and (0, $c^*/2$) wave vectors, respectively.

For our purpose, the xz and yz orbitals are equivalent so that only one set will be considered. The two lower combinations at Γ are shown in **16a** and **16b**. As for the x^2-y^2 crystal orbitals, the only difference lies in one O_{in} and one O_{sh} additional contribution in **16b**. This is also the difference between any two successive levels. Note, however, that the overlap is different from that in **15**. We will denote the presence of an oxygen p contribution with this kind of overlap as y' or Y'. Just by inspection of the three equivalent t_{2g} orbitals of an octahedron, it is clear that the strength of an antibonding interaction of this type is one-half that of the perfect π-type, that is, $y' = y/2$ and $Y' = Y/2$.[51] Thus, the difference between **16a** and **16b** (as well as between any pair of adjacent xz or yz levels at Γ) is $2Y' = Y$. Moving from Γ to X, four apical interactions are switched on and consequently all of the bands raise as much as $4Y$. The two lower crystal orbitals at Z are those shown in **17a** and **17b**. It is immediately seen that the number of antibonding contributions is exactly the same in Γ and Z so that the bands should lie at the same energy. The same result applies to all other xz and yz bands.

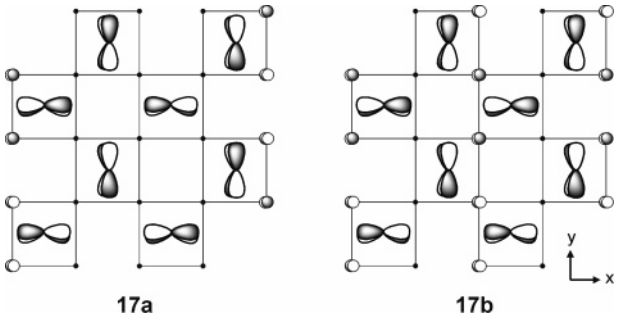

17a **17b**

With this kind of reasoning, the qualitative band structure of Figure 7a can be drawn. Again, this qualitative diagram is in excellent agreement with the extended Hückel complete band structure (see Figure 7b). Thus, this simple approach also provides a way to rationalize how different structural modifications affect the t_{2g}-block band structure in this system. According to this simple approach, the salient difference between the layers of the R−P or D−J phases is that the t_{2g}-block is now made of a series of 1D bands only. However, the x^2-y^2 bands are 1D along the c-direction, whereas the xz and yz bands are also 1D but along the a-direction. The FS for many electron counts will result from the superposition of 1D contributions along

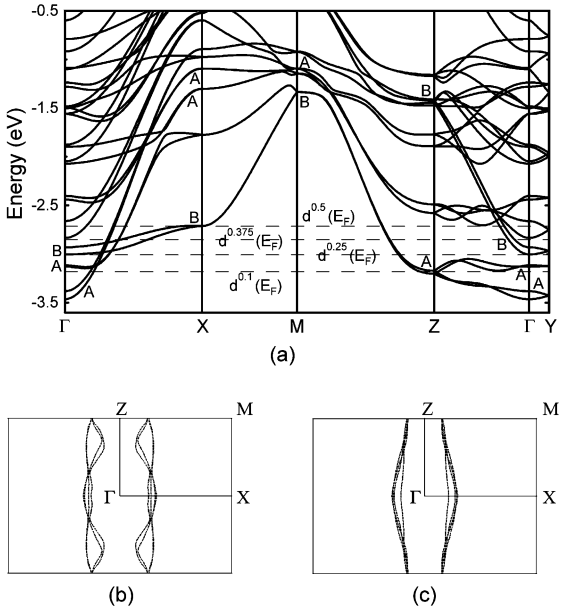

Figure 8. (a) Band structure calculated for the room-temperature structure of $Sr_2Ta_2O_7$. FS (section $k_y = 0$) calculated for the room temperature (b) and 123 K (c) structures of $Sr_2Ta_2O_7$ assuming a band filling corresponding to $d^{0.23}$ and $d^{0.2}$, respectively. The Γ, *X*, *Y*, *Z*, and *M* labels refer to the (0, 0, 0), (*a**/2, 0, 0), (0, *b**/2, 0), (0, 0, *c**/2), and (*a**/2, 0, *c**/2) wave vectors, respectively.

orthogonal directions as in the systems exhibiting the so-called hidden nesting,[51,54] and this brings about interesting possibilities if these levels may be partially filled.

G. First-Principles Results for Quadruple Layer Systems of the $A_nB_nO_{3n+2}$ Phases. Here, we report first-principles calculations for $Sr_2Ta_2O_7$, which is one of the members of this series with $n = 4$ and for which two structures are known, before (298 K) and after (123 K) the ferroelectric transition at 196 K.[49] Thus, how much the distortions occurring in these phases can affect the simple picture may be tested using this material. We will restrict ourselves to this aspect, and we will not consider here the details of the ferroelectric transition. We have also studied the room temperature, ferroelectrically distorted phase of $Sr_2Nb_2O_7$, in which the octahedral distortions are even stronger. The calculated band structure for the room-temperature structure of $Sr_2Ta_2O_7$ is shown in Figure 8a. Let us note that the unit cell contains two layers and thus all bands appear in pairs. Although at first sight this band structure may look complex, in fact it is not. After taking into account some weakly avoided band crossings and realizing that the equivalence of the *xz* and *yz* orbitals is lost in the real systems, it is quite clear that all major features of the qualitative band structure are also present here. To help the reader, we have noted with A and B labels the lower pairs of bands originating from the *xz*/*yz* and x^2-y^2 orbitals, respectively. We have also included the Fermi levels appropriate for different Ta average configurations according to a rigid band scheme. Shown in Figure 8b is a section of the FS corresponding to a $d^{0.23}$ average configuration. This section contains two pairs of open contributions, one of which is flat (1D) and the other exhibiting a slight warping (pseudo 1D), perpendicular to the *a**-direction. Thus, for this electron filling the system would behave as a 1D material along the *a*-direction. The systematic study of the FS as a function of the electron filling shows that the 1D bands along the orthogonal direction start to be filled for electron fillings slightly larger than those corresponding to $d^{0.25}$, although only for larger fillings ($\sim d^{0.5}$) are the open lines perpendicular to the *c**-direction fully developed.

When the system undergoes the ferroelectric transition, the more noticeable change is a movement of the Ta atoms in the equatorial plane so that one $M-O_{equatorial}$ distance becomes short. As a result, the x^2-y^2 orbitals are destabilized and the corresponding bands (i.e., bands B in Figure 8a) are raised in energy. As a consequence, the B-type bands start to be filled for higher band fillings ($d^{0.37}$) and the x^2-y^2 orbitals mix into the lower bands in an even smaller way. The section of the FS is now even more clearly 1D (see Figure 8c). For the $Sr_2Nb_2O_7$ compound where the distortions are even stronger,[47] the x^2-y^2 bands are even higher lying and start to be filled for slightly larger band fillings ($d^{0.4}$). It is clear that even if the octahedra in these phases are quite different from the ideal ones used in our simple qualitative scheme, the main features of the band structure are kept. Thus, we conclude that, except if the octahedral distortions are weak, partial filling of the t_{2g}-block bands by partial cationic substitution for instance will generally lead to 1D metallic systems along the *a*-axis.

At this point, let us note that phases such as $Sr_{3.2}La_{0.8}Nb_4O_{14}$ (i.e., a phase with $n = 4$ and $d^{0.2}$) or $Sr_5Nb_5O_{17.05}$ (i.e., a phase with $n = 5$ and $d^{0.18}$) have been recently found to be quasi-1D metals along the *a*-direction,[45,53] as predicted by the simple model. In previous theoretical works,[23] the unexpected 1D behavior of the last phase was attributed to specific octahedral distortions of the layer. However, the present work clearly shows that this is not the case. The 1D behavior is also exhibited by a perfectly ideal layer, and consequently it is only related to the topology of the lattice and the nature of the t_{2g} orbitals as analyzed in the previous section. Understanding the fine details of the physical behavior of these phases depends of the real degree of band filling and the relative position of the bottom part of the lower x^2-y^2 bands, which can give some additional small pockets. However, this goes beyond the scope of the present work and will not be discussed here.[55] It would be interesting to see if the 1D character along the second, orthogonal direction, associated with the x^2-y^2 orbitals, could be activated and forced to play a clear role in some of these compounds. According to our study, only for systems with regular octahedra can this become a likely possibility. Thus, it could be worth exploring if vanadium phases of this type could be prepared.

Concluding Remarks

The main goal of this work was to develop a simple yet rigorous approach that could give a feeling on the nature of the partially filled t_{2g}-block bands of different layered perovskites. We believe that the orbital approach presented above, which has been validated by first-principles calculations for many of these phases, fulfills this goal. The more relevant results of this approach are as follows: (1) There are both 1D and 2D bands near the Fermi level for the R−P and D−J phases where the bottom t_{2g}-block bands are partially filled.[20b] (2) Double layer

(54) (a) Whangbo, M.-H.; Canadell, E.; Foury, P.; Pouget, J. P. *Science* **1991**, *252*, 96−98. (b) Canadell, E.; Whangbo, M.-H. *Int. J. Mod. Phys. B* **1993**, *7*, 4005−4043. (c) Seo, D.-K.; Liang, W.; Whangbo, M.-H.; Zhang, Z.; Greenblatt, M. *Inorg. Chem.* **1996**, *35*, 6396−6400.

(55) Tobias, G.; Canadell, E., work in progress.

R−P and D−J phases of this type are generally expected to exhibit 2D metallic behavior. The 1D bands may play a role, however, for systems with regular octahedra and electron counts corresponding to $d^{0.5}$ or higher. (3) For triple layer R−P and D−J phases, the 1D bands may play a larger role for lower d electron counts than they do for the double layer phases if there are no strong octahedral apical distortions in the outer layers. Systems with such distortions will generally be 2D metals with little difference in the electron population for the inner and outer layers. (4) Even if they are structurally 2D materials, a 1D metallic behavior is expected for low t_{2g}-block band fillings of the $A_nB_nO_{3n+2}$ phases.

An important feature that must be taken into account for some of the systems in which the t_{2g}-block bands exhibit low band fillings is disorder. For low band fillings, that is, low density of carriers, an electron localization due to disorder can occur (Anderson localization[56]) in which case the conductivity would be activated. There are several possible causes of disorder in these layered perovskites in addition to the possible oxygen nonstoichiometry. First, cationic disorder occurs within the van der Waals gap either because of the intercalation or because of partial occupation with different cations of the holes between the perovskite layers. A typical example of activated conductivity due to this type of disorder is provided by the $Na_{2-x+y}Ca_{x/2}La_2Ti_3O_{10}$ ($x = 1.22$, $y = 0.32$) phase obtained from $Na_2La_2Ti_3O_{10}$.[16] Second, there is disorder in the occupation of the cation sites within the perovskite slabs. For instance, this occurs in the quadruple layer phases $Na_2Ca_2Nb_4O_{13}$ or $RbCa_2NaNb_4O_{13}$.[14,57] Because disorder lies within the slab, it may have a stronger influence than in the previous case. For instance, it is not clear if this feature may be at the origin of the absence of superconductivity in the quadruple layer D−J phase $Li_xKCa_2NaNb_4O_{13}$.[11d] Related materials in which disorder can have a decisive role in imposing the nature of conductivity are perovskite-type layered oxynitrides. Although use of a rigid band scheme and the present qualitative approach may be more questionable in this case where disorder affects the octahedral network, it may give some useful hints. The single layer R−P oxynitrides $Sr_2NbO_{4-x}N_x$ ($x \approx 0.72$),[12] and $La_xSr_{2-x}NbO_3N$ ($x \approx 0.2$),[58] possess Nb with an average $d^{0.28}$ and $d^{0.2}$ configuration, respectively. For the first of these phases, the neutron Rietveld refinement has clearly proved that the nitrogen atoms occur in the equatorial positions.[12b] This is an especially bad situation in which to expect metallic conductivity because the lower lying levels for this materials are based on the *xy* orbitals, which lie in the equatorial plane. Thus, the O/N disorder must completely kill the possibility of metallic behavior. The simple qualitative scheme suggests that this will be the general case for these layered oxynitrides. However, it also gives a hint that maybe there is a possibility of realizing the metallic behavior in these materials if the nitrogen atoms occupy the apical positions, as it has been reported for Nd_2AlO_3N.[59]

Acknowledgment. This work was supported by DGI-Spain (Projects BFM2003-03372-C03 and MAT2002-00439) and Generalitat de Catalunya (Projects 2001 SGR 333 and 2005 SGR 683). G.T. acknowledges support from the Ministerio de Ciencia y Tecnología of Spain. Some of the computations described in this work were carried out using the resources of CESCA and CEPBA.

Supporting Information Available: Two figures showing calculated extended Hückel band structures. This material is available free of charge via the Internet at http://pubs.acs.org.

JA0572755

(56) Stoneham, A. M. *Defects and Defect Processes in Nonmetallic Solids*; John Wiley: New York, 1995.
(57) Chiba, K.; Ishizawa, N.; Oishi, S. *Acta Crystallogr., Sect. C* **1999**, *55*, 1041−1043.
(58) Tobias, G. Ph.D. Thesis, Bellaterra, 2004; http://www.tdx.cesca.es/TDX-0131105-171937/.
(59) (a) Marchand, R.; Champetier, G. *C. R. Acad. Sci. Paris C* **1976**, *282*, 329−331. (b) Marchand, R.; Pastuszak, R.; Laurent, Y.; Roult, G. *Rev. Chim. Miner.* **1982**, *19*, 684−689.